PCCP

Accepted Manuscript

ROYAL SOCIETY OF CHEMISTRY

www.rsc.org/pccp

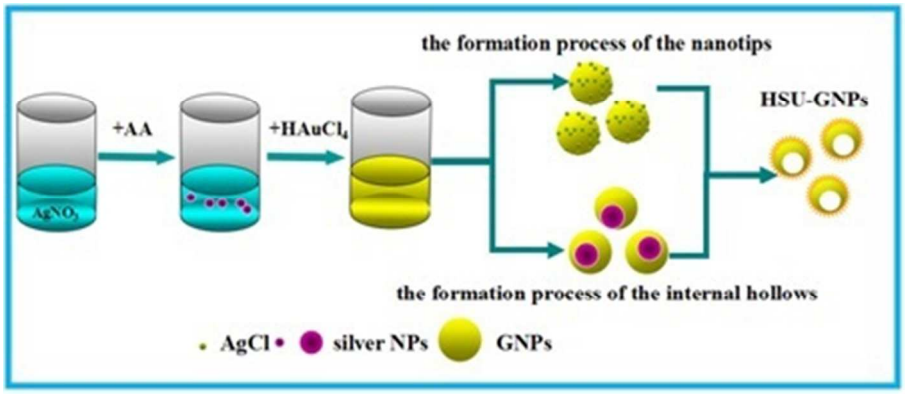

A hollow sea urchin gold nanoparticles with distinctive optical properties was prepared through a one-step galvanic replacement strategy.
95x41mm (120 x 120 DPI)

Journal Name

Cite this: DOI: 10.1039/c0xx00000x

www.rsc.org/xxxxxx

ARTICLE TYPE

Controllable synthesis and SERS characteristic of hollow sea urchin gold nanoparticles

Junpeng Li,[a] Jun Zhou,*[a] Tao Jiang,[a] Binbing Wang,[a] Min Gu,[b] Lucia Petti[c] and Pasquale Mormile[c]

Received (in XXX, XXX) Xth XXXXXXXXX 201X, Accepted Xth XXXXXXXXX 201X

DOI: 10.1039/b000000x

A hollow sea urchin gold nanoparticles (HSU-GNPs) was successfully prepared through a novel one-step galvanic replacement strategy, and their corresponding optical properties was studied in detail. During the synthesis process, the sizes of the interior hollows of the HSU-GNPs could be changed by adjusting the amount of silver nitrate added into hydrogen tetrachloroaurate trihydrate solution. The absorption spectra of the HSU-GNPs showed that the localized surface plasmon resonance (LSPR) peaks occurred red-shifts with increasing the sizes of interior hollows in the HSU-GNPs. When the added amount of silver nitrate was up to 6 μl, the LSPR peak of the synthesized HSU-GNP arrived to 726 nm as a maximum red-shift. Furthermore, the absorption spectra of the HSU-GNPs with different morphologies were theoretically simulated by the finite element method, which was consisted with the experimental results and explained the origin of red-shifts of the LSPR peak. In addition, the surface-enhanced Raman scattering (SERS) of the sea urchin gold nanoparticles were also investigated by using 4-mercaptobenzoic acid as a Raman reporter molecule. Both the experimental and calculated results showed that the HSU-GNPs had stronger SERS enhancement than that of the solid sea urchin gold nanoparticles. Especially, the HSU-GNPs prepared by adding 6 μl silver nitrate exhibited the maximum SERS enhancement factor EF = 1.1×10^9 , due to its LSPR peak at 726 nm which is near to the excitation wavelength 785nm. This feature is significant for designing the biosensor with a super-high sensitivity based on the morphology of the HSU-GNPs.

1. Introduction

As we known, the noble metal nanoparticles (NPs) have special optic properties and are widely applied into the fields of physics, chemistry, biology and life science.[1-8] As a power optical functional material, the localized surface plasmon resonance (LSPR) of the noble metal NPs are closely related to their structure parameters, including sizes, shapes, compositions, and morphologies.[9-11] Thus, the controllable synthesis of noble metal NPs is a very interesting topic and much effort has been devoted to develop available methods to create an amount of metal nanostructures, such as the hydrothermal method, the galvanic replacement method, the oil/water interface method and the template method.[12-15] It is an essential that the noble metal NPs with special structures are prepared to fully manipulate their distinctive LSPR properties. In particular, great study has been diverted to design novel hollow noble metal nanostructures due to their high active surface to volume ratio and fascinating applications in numerous areas of optoelectronic imaging, catalysis, environmental monitoring, biosensing, diagnosis and drug delivery.[16-20]

On the other hand, surface-enhanced Raman scattering (SERS) has attracted a mass of attentions because the Raman signal can usually be enhanced by several orders of magnitude for target molecules attached on the noble metal surfaces.[21,22] The generation mechanism of SERS is widely recognized as involving two major components: chemical and electromagnetic enhancement. The former one is due to an increased polarizability of the target molecules under the influence of incident radiation, as a result of which new chemical bands with the metal surface are formed.[23,24] The latter one arises from the enhancement of the electromagnetic field for the occurrence of the LSPR of nanostructured noble metal systems and is highly dependent on the matching between the excitation wavelength and LSPR band.[25,26] As a non-destructive and ultrasensitive spectroscopy analysis technique, the SERS originating from the electromagnetic enhancement is more suitable to detect the biological tissues by using the incident radiation in the "window of optical transparency", i.e., in the near infrared (NIR) spectral region of 750-1000 nm.[27, 28] Consequence, the LSPR band of the noble metal nanostructures in such a NIR region possesses obvious superiorities and promising applications for the biomedical detection.

With regard to the window of optical transparency, we hope that the structure of noble metal NPs can be tailored for satisfying the requirement of its LSPR band closed to the wavelength of incident radiation in NIR region. For example, the LSPR bands of solid spherical gold NPs (GNPs) can be tuned as much as 50

nm around 520 nm, and those bands of hollow ones can be continuously adjusted from 500 to 1000 nm by controlling the sizes of interior hollows.[29-32] Furthermore, the noble metal nanostructures with rough surfaces have a relatively high SERS intensity because of the existence of "hot spots" (a strong enhanced electromagnetic areas) on the junctions and sharp tips of nanostructures,[33-35] so that the great efforts have been directed towards the fabrication of noble metal NPs with various morphologies including raspberry,[36] flower,[37] meatball,[38] star,[39] and sea urchin.[40-41] Thus, a hollow metal nanostructure with rough morphology is naturally considered to combine their merits, that is, the adjustability of LSPR band and the high SERS intensity. However, it is a complex chemical process to synthesize a hollow metal nanostructure with rough morphology. Generally, silver seeds should be firstly synthesized to build a hollow center in GNPs,[42] and then the rough morphology of the hollow GNPs are produced by using organic moleculars as the capping agents or stabilizers such as cetyltrimethylammonium bromide (CTAB),[15,43] gum arabic,[38] sodium dodecyl sulfate (SDS),[44] and gelatin protein.[45] A typical sacrifical template approach and the galvamic replacement reaction between Ag NPs and $HAuCl_4$ had been introduced to form the hollow GNPs with a urchin-like shell by the aid of ascorbic acid as reducer and polyvinylpyrrolidone (PVP) as dispersant.[46] The introducing of these organic moleculars will block the link of the target molecules on the surface of GNPs, which inevitably impairs the following SERS applications. Therefore, it is still an enormous challenge to achieve fine tailored structure of the hollow GNPs with sophisticated morphology by a green and simple synthesize process.

In this article, we demonstrate a facile and environmentally friendly galvanic replacement strategy for high-yield synthesis of hollow sea urchin gold nanoparticles (HSU-GNPs). The surface morphologies and internal hollow sizes of the HSU-GNPs were further tuned by altering the added amount of $AgNO_3$. The UV-vis-NIR absorption spectra of the HSU-GNPs with different sizes of the interior hollows were experimentally measured and exhibited the tunable red-shift characteristics of their LSPR peaks. Meantime, the formation mechanism of the HSU-GNPs was tentatively explained and the origin of LSPR red-shifts of the HSU-GNPs was theoretically analyzed by the finite element method (FEM). Lastly, the SERS property of the HSU-GNPs was investigated by applying 4-mercaptobenzoic acid (4MBA) as a Raman reporter molecule and demostrted a high SERS enhancement.

2. Experimental

2.1 Chemicals

Silver nitrate ($AgNO_3$), and hydrogen tetrachloroaurate (Ⅲ) trihydrate ($HAuCl_4 3H_2O$), were purchased from Sigma. Ascorbic acid (AA) was purchased from Bodi Chemical Reagent Co. (Tianjin, China). 4MBA were obtained from J&K Chemical. Milli-Q water (18.2MΩ cm resistivity) was used for all solution preparations. Glass wares were cleaned by aqua regia and rinsed with deionized water several times prior to the experiment.

2.2 Synthesis of HSU-GNPs

Four sets of sample solutions were prepared as follow processes: firstly, the different amount of $AgNO_3$ (2, 4, and 6 to 8 μl, 0.1M) aqueous solutions was separately injected in four glass tubes, and then, for every glass tube, 1 mL of AA (10 mM) aqueous solution and 1 mL of $HAuCl_4$ (3 mM) aqueous solution were quickly injected in turn. After the as-prepared mixed solutions being stirred for 20 seconds, the HSU-GNPs solutions were obtained and their color rapidly changed into dark blue.

To get the precipitates of HSU-GNPs, the above as-prepared sample solutions were centrifuged at 8000 rpm for 20 min. Then the resultant precipitates were washed with deionized water and absolute ethanol by centrifugation for several times to remove impurities. Finally the four samples of HSU-GNPs were respectively dispersed in 5 ml of deionized water for later experiments.

2.3 Synthesis of 4MBA-tagged HSU-GNPs

20 μl of 4MBA (1 mM) was added to the above purified sample solutions of HSU-GNPs under stirring and the resultant solutions were agitated for 5 h, respectively. Then, the mixed solutions were centrifuged at 9000 rpm for 25 min for removing unbound 4MBA molecules, and the 4MBA-tagged HSU-GNPs settled to the bottom of reactive vessels. Next, the 4MBA-tagged HSU-GNPs were dispersed in 5 ml deionised water. Lastly, the 4MBA-tagged HSU-GNPs solution were dorpped on a quartz glass and air-dried as SERS substrate for further SERS detection.

2.4 Instruments and measurement

The scanning electron microscopy (SEM) and TEM images of the HSU-GNPs were obtained by using FESEM (SU-70) at an accelerating voltage of 5 kV and TEM (JEM-2100F JEOL) at an accelerating voltage of 200 kV, respectively. The optical absorption spectra of the HSU-GNPs were recorded with a UV-vis-NIR spectrometer (Cary5000PC). The SERS properties of the HSU-GNPs were examined by using the miniature Raman spectrometer (BWS415, B&W Tek Inc.) with a 785-nm semiconductor laser as the excitation source. The measurement parameters of the Raman spectrometer were set as follow: the laser power at the sample position was 49.55 mW and the accumulation time was 5 s; The scattered radiation was collected by a 40× objective lens with numerical aperture (NA) 0.65 and dispersed by the grating of 1200 lines/mm, and then passed through a slit with 20 μm width to the charge-coupled device (CCD) (2048×2048 pixels) detector. All the analysis was performed at room temperature.

3. Results and discussion

3.1 Characterization of samples

The HSU-GNPs were synthetized by our one-step galvanic replacement method. Typical SEM and TEM images of the HSU-GNPs are shown in Fig. 1. From Fig. 1a, the average diameter of the HSU-GNPs were calculated to be 70 ± 5nm and their tips length in the range of 5-20 nm. Fig. 1b and 1c exhibited that the HSU-GNPs have distinct interior hollows with sizes ranging from 20 to 45 nm. And the yield of the HSU-GNPs synthesized with 6 μl $AgNO_3$ was counted about 80%. The chemical compositions of the HSU-GNPs were analyzed by energy-dispersive spectrometer (EDS). As shown in Fig. 1d, it clearly displays that the sample is mainly composed of metallic gold, the

elements of silver and chlorine are from the small amount of indiscerptible silver chloride (AgCl) and other elements are from the silica substrate and the derivative of AA.

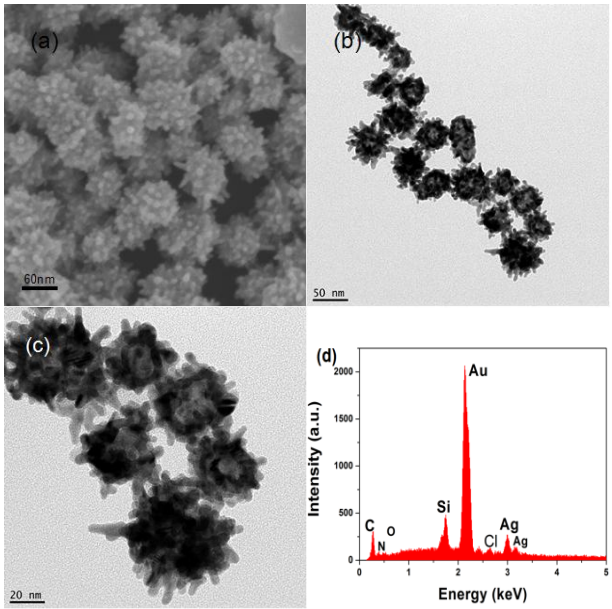

Fig. 1 (a) SEM and (b), (c) TEM images of the HSU-GNPs synthesized with 6 μl $AgNO_3$, (d) EDS of HSU-GNPs.

For insight into the formation mechanisms of the HSU-GNPs, the chemical process of the one-step galvanic replacement synthesis was illustrated in Fig. 2. Conventionally, the synthesis of sea urchin GNPs involved the template effect of the indiscerptible AgCl introduced by $AgNO_3$ in the $HAuCl_4$ aqueous solution.[46] In the initial reaction solution, Ag^+ and $AuCl_4^-$ existed as ionic state. Subsequently, the bond of Au-Cl was fractured by the adding of AA so that the Au^{3+} ions were immediately reduced into atoms to form GNPs and the released Cl^- ion combined with Ag^+ ion to produce the indiscerptible AgCl.[47] Then, AgCl would attach to the surfaces of the GNPs as new nucleation cores to further aggregate gold atoms into sea urchin morphology. However, in our synthesis process of HSU-GNPs, some of the $AgNO_3$ was firstly reduced into Ag atoms to form silver NPs by AA in a short time, and then these silver NPs were mixed with $HAuCl_4$ acting as the reduction center of gold ions. A galvanic replacement reaction between silver NPs and $HAuCl_4$ leaded to the formation of gold shell around the silver NPs and the dissolution of silver NPs with the migration of electrons. It is because the reduced gold has great tendency to nucleate on the surfaces of silver NPs for lowering the energy cost.[42] Along with the disappearance of the internal silver NPs, the outside gold shell continually shrank to minimize the surface energy until the complete dissolution of silver NPs. As a consequence, a hollow gold nanoparticle was obtained. Meanwhile, same as the above conventional method, the other unreduced Ag^+ ion combined with Cl^- ion to produce the indiscerptible AgCl as the growth director of the thorny GNPs. For understanding the role of $AgNO_3$, a control sample was also prepared by directly mixing AA and $HAuCl_4$ without adding $AgNO_3$. As shown in Fig. 3, only irregular gold nanoclusters were produced in the control sample, which further confirmed the surface-modified effect of indiscerptible AgCl as anchoring sites of the outside branches on suitable surface sites.[47]

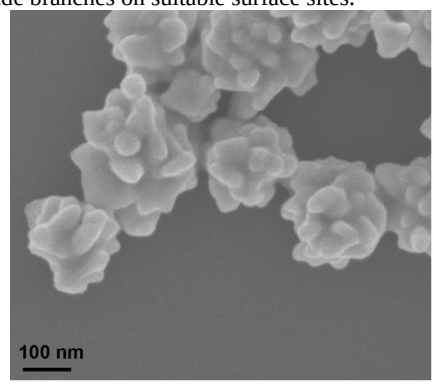

Fig. 3 The SEM image of the GNPs synthesized absence of $AgNO_3$.

According to the above analysis of the synthetic strategy, it is expected that the number of branches and the size ratio of cavity to shell can be widely tailored by controlling the amounts of $AgNO_3$. As described in section 2.2, during the preparation of HSU-GNPs, the amounts of $AgNO_3$ was selectively regulated from 2 to 8 μl with other synthetic conditions remaining unchanged. The TEM images of four samples were shown in Fig. 4. As shown in Fig. 4a, sample 1 is a sea urchin GNPs with a very littler interior hollow, which is originated from few silver NPs. From Figs. 4b and 4c, there are obvious interior hollows in sea urchin GNPs, i.e. samples 2 and 3 are HSU-GNPs, and the interior hollows grown bigger with increasing the amounts of $AgNO_3$. Comparing Fig. 4d with Fig. 4c, only a few of small hollows appear in sample 4, and the size of sea urchin GNPs is larger than that of sample 3. It is probably because that more and more spikes appeared and connected to each other to form new layer around the initial gold shell at such an added amount of $AgNO_3$. With the increasing thickness of the new outer layer, the gold shell acutely shrank to minimize the surface energy, which

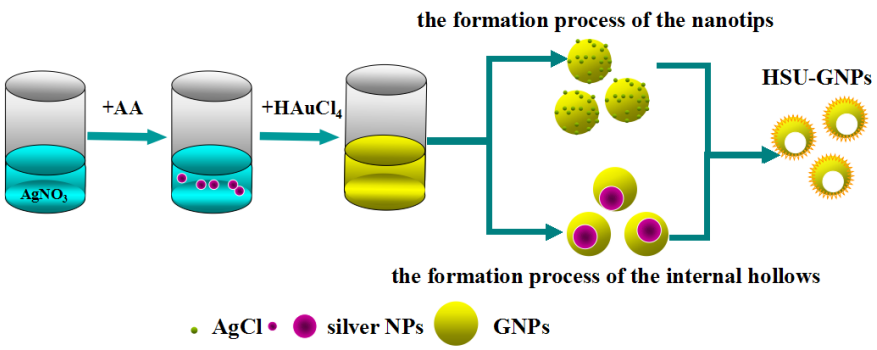

Fig. 2 The chemical process of the one-step galvanic replacement synthesis of the HSU-GNPs.

results in the obvious larger of the GNP and the smaller hollow. And the cavity size and shell thickness distributions of the HSU-GNPs obtained from various conditions are visually shown in Fig. 5. It clearly presented that the variation of size and morphology of GNPs can be controlled by the amount of $AgNO_3$ which supplied the silver NPs and indiscerptible AgCl in the reaction system. Therefore, the amount of $AgNO_3$ is the crucial factor for the generation of HSU-GNPs.

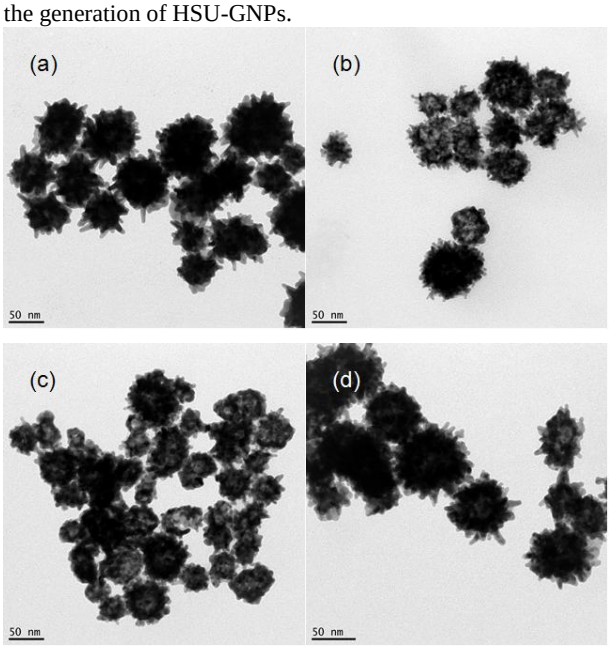

Fig. 4 TEM images of samples prepared with different amounts of $AgNO_3$. (a) Sample 1, 2 µl; (b) Sample 2, 4 µl; (c) Sample 3, 6 µl; and (d) Sample 4, 8 µl.

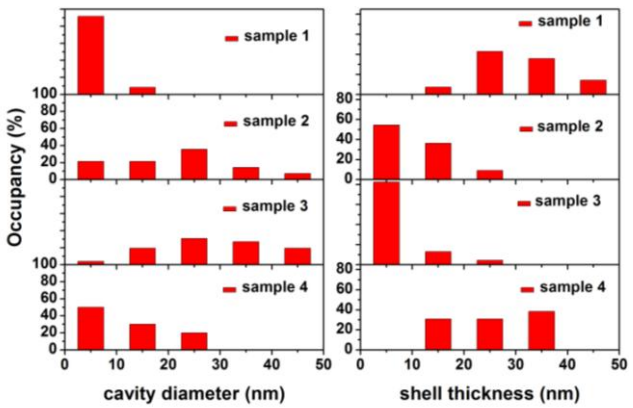

Fig. 5 The cavity size and shell thickness distributions of the different HSU-GNPs samples.

The UV-vis-NIR absorption spectra of the HSU-GNPs in aqueous solution are shown in Fig. 6. Initially, in the case without added $AgNO_3$, the main LSPR peak of the GNPs locates at 672 nm. With increasing the amount of $AgNO_3$ in the reaction solution, the LSPR peaks of the obtained GNPs gradually shift to the near infrared wavelength, which derives from the progressive formation of interior hollow and more branches on the rough surfaces of GNPs. When the amount of $AgNO_3$ arrived 6 µl, the LSPR peak moves to as far as 726 nm with a broad absorption band from 500 to 1000 nm. However, as shown in Fig. 6, adding $AgNO_3$ up to 8 µl, the LSPR peak occurs blue-shift, which presents the absorption bands of GNPs did not always sustain the red shift tendency with further increasing the amount of $AgNO_3$ due to decreasing the ratio of hollow size to shell thickness. Thus, the HSU-GNPs synthetized with 6µl $AgNO_3$ is selected as our main research objective because its LSPR peak is near the excite wavelength of the later SERS measurement.

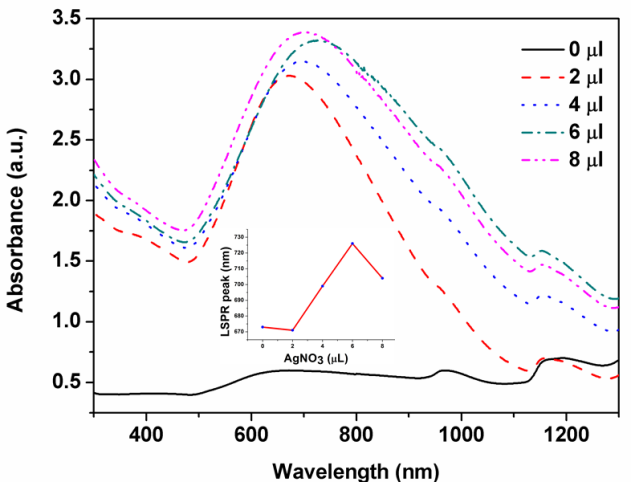

Fig. 6 UV-vis-NIR absorption spectra of GNPs in aqueous solution prepared with different amount of $AgNO_3$: 0, 2, 4, 6, and 8 µl. The inset is the dependence of LSPR peak on the amount of $AgNO_3$.

To further investigate the LSPR characteristics dependence on the structures of HSU-GNPs, the optical absorption spectra of the various sea urchin GNPs models were simulated by using the FEM software (COMSOL Multiphysics 4.1). Typically, we set the diameters of sea urchin GNPs models to be same, and their surfaces were textured with some inclined or standard spines, respectively, as illustrated in the inset of Fig. 7. In Fig. 7a, the LSPR peak of the sea urchin GNP with standard spines appears at 781 nm. But for the sea urchin GNP with inclined spines, there are a main LSPR peak at 773 nm and two smaller intensity absorption peaks around 900 nm. It is obvious that, the two smaller intensity absorption peaks can be attributed to the effect of inclined spikes which originates from the multipolar plasmon modes induced by the geometric asymmetry of the sea urchin GNP with inclined spikes.[48] Thus, for the experimental absorption spectra of the sea urchin GNPs, the small absorption shoulder peak at around 950 nm in Fig. 6 was just as the effect of inclined spikes, and the peak located at 1200 nm came from the absorption of aqueous solution. In addition, to verify the red-shift of the LSPR band of the sea urchin GNPs in Fig. 6, three HSU-GNPs with different thick nanoshells were also structured. As shown in Fig. 7b, the absorption spectrum of the HSU-GNPs with nanoshell thickness of 20nm is almost same as that of the solid sea urchin GNPs (SSU-GNPs). And, the LSPR peaks of HSU-GNPs red-shifts from 780 nm to 850 nm with decreasing the nanoshell thickness from 20 nm to 5 nm, gradually. It is confirmed that the red-shifts of the absorption bands in Fig. 6 were due to the increase of the hollow sizes in the HSU-GNPs. Actually, as we known, such red-shifts of the absorption bands of HSU-GNPs were caused by the hybridization of the simultaneously excited plasmons on the outer and inner surfaces of a metallic shell. That is, the two excited plasmons will interact

to produce a high-energy mode and a low-energy mode which are respectively corresponded to the antisymmetric coupling (antibonding) and the symmetric coupling (bonding) between the cavity and sphere plasmons.[49] When the shell becomes thinner, the interaction of the two plasmons becomes stronger and leads to a larger energy separation between the high-energy mode and the low-energy mode, as a result, a distinct red-shift of the LSPR band occurs. In contrast, for a thick nanoshell, the interaction between the two plasmons is weak and the absorption band does not obviously shift. This is the reason that the absorption spectrum of the HSU-GNP model with a larger shell thickness of 20 nm is coincided with that of the SSU-GNPs model. It should be noted that, only one sea urchin GNP module is used in these calculations. Therefore, the calculated spectra show narrow LSPR bands, which are different from the experimental results because of neglecting the interaction among the numerous sea urchin GNPs.

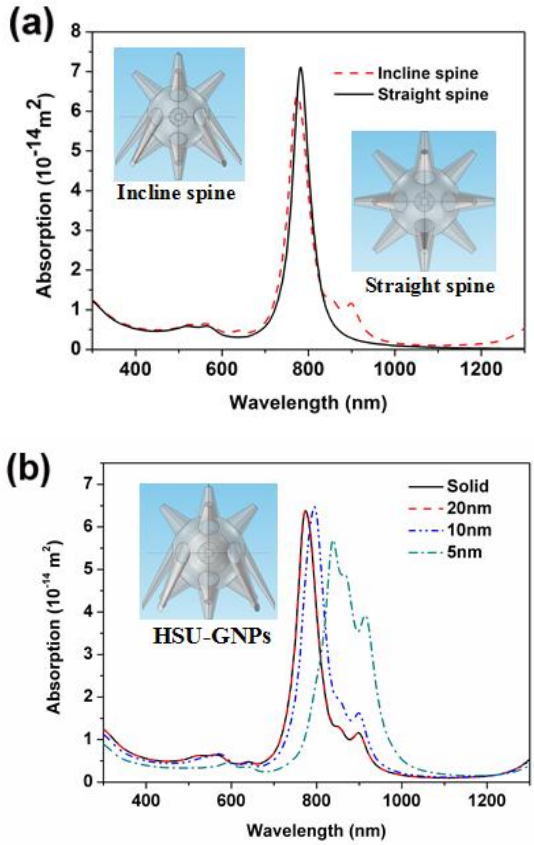

Fig. 7 Simulation absorption spectra of the sea urchin GNPs with (a) incline and standard spines and (b) different shell thickness. Inset: the models of the sea urchin GNPs for (a) incline and straight spine and (b) HSU-GNPs. All calculated models were consisted of a sphere with diameter 50 nm and sixteen spikes with length 50 nm.

The local electric field intensities around the sea urchin GNPs were calculated to evaluate their performance under irradiating of the monochromatic light at 785 nm. The permittivity data of gold are obtained from the bulk experimental result of Johnson and Christy.[50] The typical distributions of electric field strength around the SSU-GNPs and HSU-GNPs are shown in Fig. 8a and 8b, respectively. As it is anticipated, the strongest local electric field areas are observed in the vicinity of spikes and the maximums of electric field intensities are found to be 497.81 and 644.93, respectively. It was found that, the HSU-GNPs can produce an enhanced local electric field comparing with that of the SSU-GNPs, which indicates the internal hollow of HSU-GNPs is beneficial for enhancing of the local electric field due to the plasmon hybridization effect discussed above.

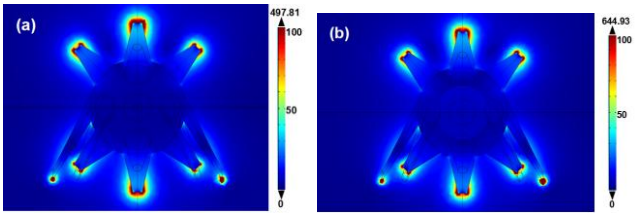

Fig. 8 FEM simulation of the electric field intensity distribution of (a) the SSU-GNPs and (b) the HSU-GNPs with a shell thickness of 10 nm. The diameters of sphere or shell in the calculated models were same as 50 nm.

3.2 SERS performance of the HSU-GNPs

The SERS performance of the HSU-GNPs was investigated by measuring the Raman spectra of 4MBA-tagged HSU-GNPs. As illustrated in Fig. 9, all the samples of 4MBA-tagged HSU-GNPs present strong characteristic bands of 4MBA due to the exceptional SERS enhancement. The two dominant peaks at 1077 and 1590 cm^{-1} are assigned to the ring breathing modes.[51] The Raman band at 845 cm^{-1} is attributed to the COO^- bending mode ($\delta(COO^-)$) and that at 1137 cm^{-1} originates from a mixed mode ($13\beta(CCC)+\nu(C\text{-}S)+\nu(C\text{-}COOH)$).[51,52] Additionally the one at 1432 cm^{-1} is ascribed to the $\nu_s(COO^-)$ stretching mode.[53] Although the positions of Raman peaks of all samples are same, their intensities are different. It is obviously observed that the intensities of Raman peaks increased first as increasing the amount of $AgNO_3$ and reached the maximum for 4MBA-tagged HSU-GNPs synthesized at 6 µl $AgNO_3$ which possessed the largest interior hollow as described in Section 2.1. Then, the SERS intensities oppositely decreased with the further increase of $AgNO_3$ due to reducing the ratio of interior hollow to shell. Thus, the SERS enhancement of sample synthesized at 6 µl $AgNO_3$ was explored in detail next.

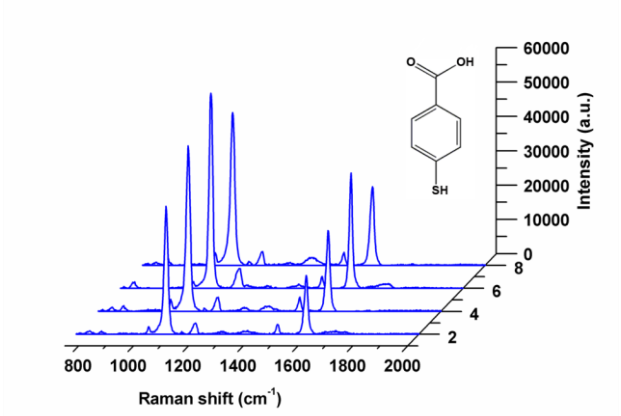

Fig. 9 Raman spectra of 4MBA on the sea urchin GNPs synthesized with different amount of $AgNO_3$: (a) 2, (b) 4, (c) 6, and (d) 8 µl.

The enhancement factor (EF), which is one of the most important parameters for the SERS effect, was calculated using the following equation:[54-56]

$$EF = (I_{SERS}/I_{bulk}) \times (N_{bulk}/N_{SERS})$$

where I_{SERS} and I_{bulk} are the intensities of the same Raman band in the SERS and bulk Raman spectra, respectively; N_{bulk} is the number of bulk molecules probed in the bulk sample; and N_{SERS} is the number of molecules adsorbed on the SERS substrate. Here, the SERS intensity of the peak at 1076 cm^{-1} was used to roughly calculate the EF value. The Raman spectrum of the 4-MBA solution (10 mM) was used to estimate the "bulk" values of the EF. N_{bulk} was calculated by using a 4MBA solution concentration at 10 mM and the focal volume of the laser in the Raman system. The diameter of the illumination focus 1.473 μm was first calculated using the following equation: Ddiameter = (λ/NA) × 1.22,[57] in which the NA of the objective lens of the Raman spectrometer was 0.65 and the wavelength of the excitation laser was 785 nm; besides, the penetration depth of 785 nm laser beam is about 2 μm in the solutios. Then, the illuminated volume was 1.66 μm^3, and the $N_{bulk} = 1\times10^{13}$. To obtain the value of N_{SERS}, with the same diameter of the illumination focus 1.473 μm, $N_{SERS} = 2.3\times10^5$ was obtained by dropped 100 μl diluted 4MBA-tagged HSU-GNPs solution on a quartz glass with diameter 1.5 cm. In addition, as shown in Fig. 10, the I_{bulk} and I_{SERS} (synthesized with 6 μl $AgNO_3$) values (the laser power was 49.55 mW and the accumulation time was 5 s) were 4.27×10^4 and 1.08×10^6, respectively. Thus, the EF value of the SERS substrate was calculated as $EF_{sample3} = 1.1\times10^9$. For other samples of the HSU-GNPs synthesized with 2, 4, and 8 μl $AgNO_3$, the calculated EF are $EF_{sample1} = 7.5\times10^8$, $EF_{sample2} = 1.03\times10^9$ and $EF_{sample4} = 1.02\times10^9$, respectively.

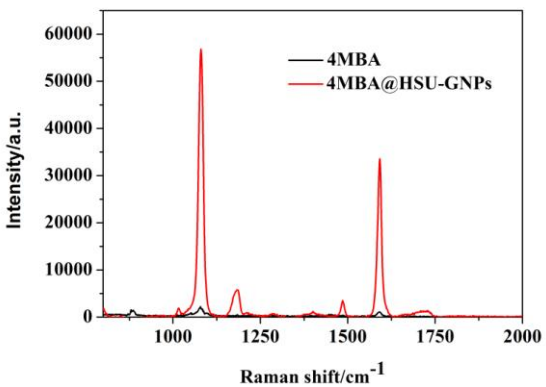

Fig. 10 The SERS spectrum of 4MBA collected from the normal Raman spectrum of 4MBA in solution and the 4MBA-tagged HSU-GNPs under the same sampling conditions.

The reproducibility of the SERS signal of the 4MBA-tagged HSU-GNPs was also ivestigated by randomly choosing ten probe sites on the SERS substrates. As shown in Fig.11a, the difference among the ten SERS signal intensity is small. These results demonstrated the excellent SERS reproducibility of the SERS substrate. To evaluate the time stability of the SERS signal, the Raman spectra of the 4MBA-tagged HSU-GNPs were measured at differnet time intervals and shown in Fig. 11b. It clearly displayes the nice time stability of the SERS substrate.

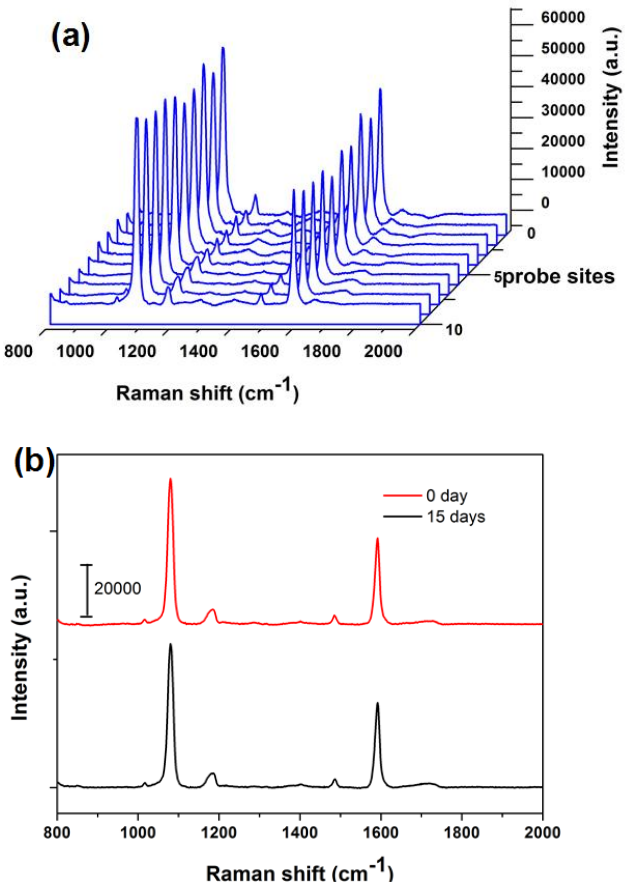

Fig. 11 The Raman spectra of the 4MBA-tagged HSU-GNPs (a) at diffenent prob sites on the SERS substrat, and (b) at differnet time intervals for the same SERS substrates.

According to the above calculated values of EF, the HSU-GNPs exhibited a high SERS performance. It stems not only from the much higher surface roughness caused by spikes on the surface of GNPs but also the interior hollow in the HSU-GNPs. In fact, as analyzed in section 3.1, the strongest enhanced localized electric field areas can be found in the vicinity of the tips of spikes, which were called as "hot spots" to excite SERS up to a higher EF. On the other hand, by comparing the EF values of the four samples, we found that, the larger the ratio of interior hollow size to shell thickness the larger the SERS EF values of the HSU-GNPs. The main reason was the better matching of the LSPR band of the HSU-GNPs with the excitation wavelength, which is consistent with the results simulated by FEM before.

4. Conclusions

In conclusion, we have developed a facile one-step method to synthesize sea urchin GNPs with interior hollows for SERS application. The sizes of the internal cavity as well as the morphologies of the HSU-GNPs can be tuned by altering the added $AgNO_3$ amount. According to the galvanic replacement synthesis process, the formation mechanism of the HSU-GNPs is discussed. Compared the method based on silver seed, the proposed one-step reaction method is very promising for synthesizing HSU-GNPs. In addition, the UV-vis-NIR absorption spectra of the HSU-GNPs in aqueous solution exhibit that the

main absorption peaks can be shifted to as far as 726 nm by adjusting the ratio of interior hollow size to shell thickness. The absorption spectra of the HSU-GNPs are numerically simulated by FEM for exploring the reason of the red-shifts in the experimental absorption spectra. Furthermore, both the experimental and modulation results show the SERS enhancement capability of the HSU-GNPs is much better than that of the SSU-GNPs. Therefore, the HSU-GNPs have a high superiority in SERS applications, which is of great importance to the development of highly sensitive immunoassay.

Acknowledgement

This work was supported by the National Natural Science Foundation of China (NSFC) (Grant Nos. 61275153, 61320106014 and 11404177); the Natural Science Foundation of Zhejiang (Grant No. LY12A04002); the International Collaboration Program of the Natural Science Foundation of Ningbo (Grant Nos. 2010D10018 and 2012A610107), and K. C. Wong Magna Foundation of Ningbo University, China. Min Gu acknowledges the support from the Australian Research Council Laureate Fellowship program (FL100100099) and from the Science and Industry Endowment Fund.

Notes and references

[a] *Institute of Photonics, Faculty of Science, Ningbo University, Ningbo 31†5211, Zhejiang, China Tel: +86-574-87600794; Fax: +86-574-87600744; E-mail: zhoujun@nbu.edu.cn*

[b] *Centre for Micro-Photonics, Faculty of Science, Engineering and Technology, Swinburne University of Technology, Hawthorn, VIC 3122, Australia*

[c] *Institute of Cybernetics "E. Caianiello" of CNR, Via Campi Flegrei 34, 80072 Pozzuoli, Italy*

1 M. I. Stockman, Opt. Express, 2011, **19**, 22029-22106.
2 J. Homola, Chem. Rev., 2008, **108**, 462-493.
3 T. W. Ebbesen, H. J. Lezec, H. F. Ghaemi, T. Thio, P. A. Wolff, Nature, 1998, **391**, 667-669.
4 R. M. Jarvis, R. Goodacre, Chem. Soc. Rev., 2008, **37**, 931-936.
5 D. Pissuwan, C. H. Cortie, S. M. Valenzuela, M. B. Cortie, Trends Biotechnol, 2010, **28**, 207-213.
6 Z. Liu, L. Cheng, L. Zhang, Z. B. Yang, Z. Liu, J. X. Fang, Biomaterials., 2014, **35**, 4099-4107.
7 J. L. Li, D. Day, M. Gu, Adv. Materials., 2008, **20**, 3866-3811.
8 P. Zijlstra, J. W. M. Chon, M. Gu, Nature, 2009, **459**, 410-413.
9 C. L. Nehl, J. H. Hafner, J. Mater. Chem., 2008, **18**, 2415-2419.
10 K. E. Lee, A. V. Hesketh, T. L. Kelly, Phys. Chem. Chem. Phys., 2014, **16**, 12407-12414.
11 C. Noguez, J. Zhang, J. Phys. Chem. A, 2009, **113**, 4068-4074.
12 C. Yang, X. T. Su, F. Xiao, J. K. Jian, J. D. Wang, Sensors and Actuators B.; 2011, **158**, 299-303.
13 J. Han, Y. Liu, R. Guo, Adv. Funct. Mater., 2009, **19**, 1112-1117.
14 H. C. Zeng, Current Nanoscience, 2007, **3**, 177-181.
15 H. J. You, Y. T. Ji, L. Wang, S. C. Yang, Z. M. Yang, J. X. Fang, X. P. Song, B. J. Ding, J. Mater. Chem., 2012, **22**, 1998-2006.
16 J. Zeng, Q. Zhang, J. Chen, Y. Xia, Nano Lett. 2010, **10**, 30-35.
17 N. D. Zhang, F. Xiao, J. Bai, Y. J. Lai, J. Hou, Y. Z. Xian, L.T. Jin, Talanta, 2011, **87**, 100-105.
18 Y. Xia, W. Li, C.M. Cobley, J. Chen, X. Xia, Q. Zhang, M. Yang, E. C. Cho, P. K. Brown, Acc. Chem. Res., 2011, **44**, 914-924.
19 J. Hu, M. Chen, X. Fang, L. Wu, Chem. Soc. Rev., 2011, **40**, 5472-5491.
20 Y. Hu, Q. Chen, Y. Ding, R. Li, X. Jiang, B. Liu, Adv. Mater., 2009, **21**, 3639-3643.
21 J. N. Anker, W. P. Hall, Nat. Mater., 2008, **7**, 442-453.
22 D. C. Rodrigues, G. F. S. Andrade and M. L. A. Temperini, Phys. Chem. Chem. Phys., 2013, **15**, 1169-1176.
23 Y. N. Xia, Y. J. Xiong, B. Lim, S. E. Skrabalak, Angew. Chem, 2009, **48**, 60.
24 Y. C. Liu, Langmuir., 2002, **18**, 174-181.
25 M. T. Sun, S. S. Liu, M. D. Chen, H. X. Xu, J. Raman Spectrosc., 2009, **40**, 137-143.
26 M. Gellner, B. Küstner, S. Schlücker, Vibrational Spectroscopy., 2009, **50**, 43-47.
27 S. Jeong, N. Won, J. Lee, J. Bang, J. Yoo, S. G. Kim, J. A. Chang, J. Kim, S. Kim, Chem. Commun., 2011, **47**, 8022-8024.
28 J. C. Zhou, Z. L. Yang, W. Dong, R. J. Tang, L. D. Sun, C. H. Yan, Biomaterials, 2011, **32**, 9059-9067.
29 Y. G. Sun, Y. N. Xia, J. Am. Chem. Soc., 2004, **126**, 3892-3901.
30 X. Lu, H. Y. Tuan, J. Chen, Z. Y. Li, B. A. Korgel, Y. N. Xia, J. Am. Chem. Soc., 2007, **129**, 1733-1742.
31 D. Schebarchov, B. Auguié and E. C. Le RuD, Phys. Chem. Chem. Phys., 2013, **15**, 4233-4242.
32 D. Aherne, M. Gara, J. M. Kelly, Y. K. Gun'ko, Adv. Funct. Mater., 2010, **20**, 1329-1338.
33 J. Fang, S. Du, S. Lebedkin, Z. Li, R. Kruk, M. Kappes and H. Hahn, Nano Lett., 2010, **10**, 5006-5013.
34 X. Tang, W. Cai, L. Yang and J. Liu, Nanoscale, 2014, **6**, 8612-8616.
35 H. Liu, Z. Yang, L. Meng, Y. Sun, J. Wang, L. Yang, J. Liu and Z. Tian, J. Am. Chem. Soc., 2014, **136**, 5332–5341.
36 S. Guo, S. Dong, E. Wang, Cryst. Growth Des., 2008, **8**, 3581-3585.
37 S. Cherevko, C. H. Chung, Sens. Actuators B, 2009, **142**, 216-223.
38 H. Wang, N. J. Halas, Adv. Mater., 2008, **20**, 820-825.
39 W. Moukarzel, J. Fitremann, J. Marty, Nanoscale, 2011, **3**, 3285-3290.
40 B. V. Broek, F. Frederix, K. Bonroy, H. Jans, K. Jans, G. Borghs, G. Maes, Nanotechnology, 2011, **22**, 015601.
41 J. Li, J. Wu, X. Zhang, Y. Liu, D. Zhou, H. Z. Sun, H. Zhang, B. Yang, J. Phys. Chem. C, 2011, **115**, 3630-3637.
42 N. Ortiz, S. E. Skrabalak, Crys. Growth Des., 2011, **11**, 3545-3550.
43 S. H. Chen, Z. L. Wang, J. Ballato, S. H. Foulger, D. L. Carroll, J. Am. Chem. Soc., 2003, **125**, 16186-16187.
44 C. H. Kuo, M. H. Huang, Langmuir, 2005, **21**, 2012-2016.
45 L. H. Lu, K. L. Ai, Y. Ozaki, Langmuir, 2008, **24**, 1058-1063.
46 W. Wang, Y. Pang, J. Yan, G. Wang, H. Suo, C. Zhao, S. Xing, Gold Bull., 2012, **45**, 91-98.
47 H. Yuan, W. H. Ma, C. C. Chen, J. C. Zhao, J. W. Liu, H. Y. Zhu, X. P. Gao, Mater. Chem., 2007, **19**, 1592-1600.
48 D. J. Wu, J S. M. iang, Y. C, X. J. Liu, Opt. Express., 2012, **20**, 26559-26567.
49 E. Prodan, P. Nordlander, J. Chem. Phys., 2004, **120**, 5444-5454.
50 P. B. Johnson, R. W. Christy, Phys. Rev. B, 1972, **6**, 43-70.
51 A. Michota, J. Bukowska, J. Raman Spectrosc., 2003, **34**, 21-25.
52 Y. J. Kwon, D. H. Son, S. J. Ahn, M. S. Kim, K. Kim, J. Phys. Chem., 1994, **98**, 8481-8487.
53 M. Wells, D D. L. ermody, H. C. Yang, T. Kim, R. M. Crooks, A. J. Ricco, Langmuir, 1996, **12**, 1989-1996.
54 E. C. L. Ru, E. Blackie, M. Meyer and P. G. Etchegoin, J. Phys. Chem. C, 2007, **111**, 13794-13803.
55 G. Hong, C. Li and L. Qi, Adv. Funct. Mater., 2010, **20**, 3774-3783.
56 Y. He, S. Su, T. T. Xu, Y. L. Zhong, J. A. Zapien, J. Li, C. H. Fan, S. T. Lee, Nano Today, 2011, **6**, 122–130.
57 S. P. Xu, X. H. Ji, W. Q. Xu, X. L. Li, L. Y. Wang, Y. B. Bai, B. Zhao, Y. Ozaki, Analyst, 2004, **129**, 63–68.